

# Inertia compensation scheme for wind turbine simulator based on deviation mitigation

Weijie LI<sup>1</sup>, Minghui YIN<sup>1</sup>, Zaiyu CHEN<sup>1</sup>, Yun ZOU<sup>1</sup>



**Abstract** Wind turbine simulator (WTS) is an important test rig for validating the control strategies of wind turbines (WT). Since the inertia of WTSs is much smaller than that of WTs, the inertia compensation scheme is usually employed in WTSs for replicating the slow mechanical behavior of WTs. In this paper, it is found that the instability of WTSs applying the inertia compensation scheme, characterized by the oscillation of compensation torque, is caused by the one-step time delay produced in the acceleration observation. Hence, a linear discrete model of WTS considering the time delay of acceleration observation is developed and its stability is analyzed. Moreover, in order to stably simulate WTs with large inertia, an improved inertia compensation scheme, applying a first-order digital filter to mitigate deviation response induced by the time

delay, is proposed. And, the criterion for selecting the filter coefficients is established based on the stability condition analysis. Finally, the WTS with the proposed scheme is validated by simulations and experiments.

**Keywords** Wind turbine simulator, Inertia compensation scheme, Stability analysis, Deviation mitigation

## 1 Introduction

Along with the rising concern about serious energy crisis and environmental pollution, the wind power generation technologies have gained comprehensive attention in recent decades. With regard to the performance test of control strategies for wind energy conversion systems (WECS), the experiments on field wind turbines (WT) are costly and unrepeatably. Therefore, wind turbine simulators (WTS) have become necessary and convenient tools for preliminary experiments.

A WECS mainly consists of the electric system and aero-mechanical system, which are usually dissociated and studied separately [1–3]. Correspondingly, there are also two types of WTS systems built in the current literatures. On the one hand, the grid-connection and the electric power quality are focused [4–8]. On the other hand, Reference [9–21] concern the aero-mechanical dynamics to provide a performance test rig for WT control strategies. This paper will focus on the latter type.

Because the slow dynamics of WTs resulted from high rotor inertia is one of key issues in the control strategy design of WTs [1, 2, 22, 23], the WTS should replicate the mechanical behavior similar to field WTs [9–20]. However, the moment of inertia of WTSs is usually much smaller than that of WTs, and therefore the inertia

CrossCheck date: 15 February 2016

Received: 12 July 2015 / Accepted: 15 February 2016 / Published online: 6 July 2016

© The Author(s) 2016. This article is published with open access at Springerlink.com

✉ Minghui YIN  
ymhui@vip.163.com

Weijie LI  
wikey\_lee@163.com

Zaiyu CHEN  
czy\_1989@foxmail.com

Yun ZOU  
zouyun@vip.163.com

<sup>1</sup> School of Automation, Nanjing University of Science and Technology (NJUST), Nanjing 210094, China

compensation scheme is applied to simulate the slow behavior of mechanical dynamics of WTs [10–19].

However, it has been found that when simulating a WT with large rotor inertia, the WTS applying the inertia compensation scheme might be unstable and the instability is characterized by the asymptotic divergence of compensation torque [10–12]. It is intuitively pointed out that the external noise of speed measurement in the differential-based acceleration observation used by the inertia compensation scheme is responsible for this instability, and accordingly a low-pass filter (LPF) is recommended to attenuate the interference signal [11, 12]. The similar implementation of LPF for the external noise elimination is also presented [4, 16]. Moreover, in order to avoid the differential-based acceleration observation that can easily exaggerate the external noise of speed measurement, the pseudo derivative feedback [13] and estimation of the load torque [14] are proposed which, however, increase the complexity of WTS implementation.

Different from the aforementioned literatures which focus on improving the acceleration observation by removing differentiator, in this paper such type of instability of WTS is investigated and its cause is perceived as the one-step time delay of the differential-based acceleration observation rather than the external noise of speed measurement. Furthermore, by depicting the deviation of response between WTS and WT, a deviation mitigation method, which can be easily realized by a first-order filter added in the inertia compensation scheme, is proposed and the criterion for selecting the filter coefficients is provided. Note that this filter aims to mitigate the divergent response stimulated by the time delay in acceleration observation. When employing the proposed inertia compensation scheme based on deviation mitigation, the slow dynamic behavior of WTs can be replicated stably and conveniently. Finally, both simulations and experiments are conducted to verify the proposed inertia compensation scheme.

## 2 Modeling of the WTS

As illustrated in Fig. 1, the WTS system mainly consists of two subsystems, a real-time digital control system (DCS) and a torque-controlled motor as the replaced prime mover [7–21]. With the simulation algorithm running in DCS, torque-controlled motor can mimic the aerodynamic and mechanical behavior of WTs.

### 2.1 Aerodynamic model of WT

The aerodynamic torque of WT driven by inflow wind can be expressed by:

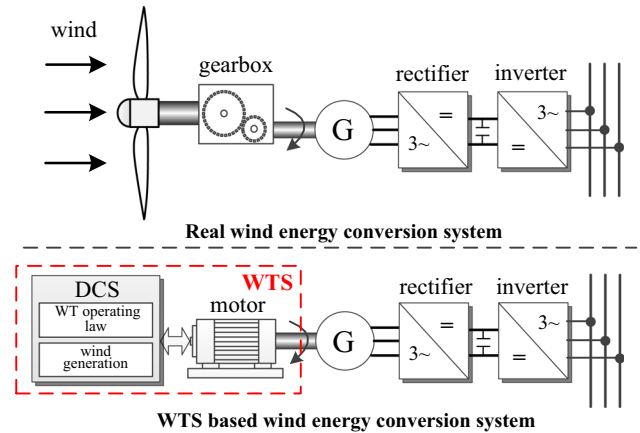


Fig. 1 Structure of the WTS-based wind energy conversion system

$$T_a = 0.5\rho\pi R^2 v^3 C_p(\lambda, \beta) / \omega_t \tag{1}$$

where  $\rho$  is the air density ( $\text{kg/m}^3$ );  $R$  is the radius of the wind turbine (m);  $v$  is the wind speed (m/s);  $\omega_t$  is the rotor speed (rad/s);  $C_p$  is the power coefficient which is a nonlinear function of the tip speed ratio (TSR) and the blade pitch angle  $\beta$ , as shown in Fig. 2. TSR  $\lambda$  is expressed as:

$$\lambda = \omega_t R / v \tag{2}$$

### 2.2 Mechanical dynamics of WT and WTS

Assuming that the main shaft and the gearbox are infinitely rigid, the drive train of WT can be regarded as a one-mass model [22]:

$$T_a/n_g - T_g = J_t \dot{\omega}_g \tag{3}$$

where  $J_t$  is the moment of inertia on high-speed shaft side of drive chain ( $\text{kgm}^2$ );  $n_g$  is the transmission ratio of

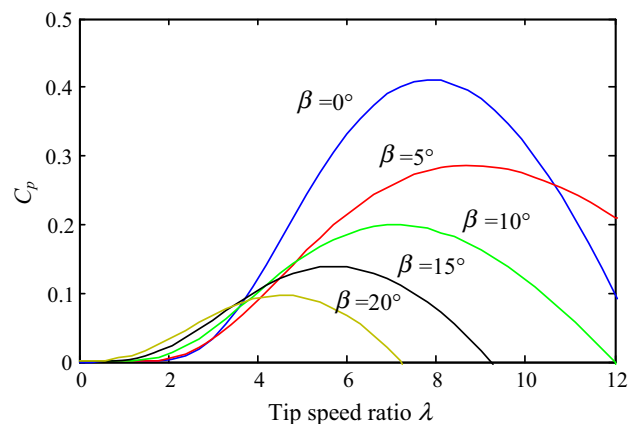


Fig. 2  $C_p$  curve as a function of TSR  $\lambda$  and the blade pitch angle  $\beta$

gearbox;  $\omega_g$  and  $T_g$  are the generator speed (rad/s) and generator torque (Nm), respectively.

Likewise, the mechanical dynamics of WTS can be expressed as:

$$T_s - T_g = J_s \dot{\omega}_s \tag{4}$$

where  $T_s$  is the motor torque produced from the prime mover (Nm);  $J_s$  is the total moment of inertia of WTS ( $\text{kgm}^2$ );  $\omega_s$  is the rotational shaft speed of WTS (rad/s).

By comparing (3) and (4), it is obvious that because the inertia of WTS  $J_s$  is much smaller than that of WT  $J_t$ , WTS cannot replicate the mechanical dynamics similar to WT even if the motor torque  $T_s$  is controlled following the aerodynamic torque  $T_a/n_g$ .

To obtain the similar mechanical dynamics, the inertia compensation scheme is employed by WTS [10–19]. By subtracting (3) from (4) based on the assumption that  $\dot{\omega}_s$  is equal to  $\dot{\omega}_g$ , the rearrangement gives:

$$T_s = T_a/n_g - (J_t - J_s)\dot{\omega}_g \tag{5}$$

where  $(J_t - J_s)\dot{\omega}_g$  represents the dynamic compensation torque  $T_{comp}$  which is calculated according to the acceleration of rotational shaft. Thus, the mechanical dynamics of the two systems would be identical if the motor torque is compensated by  $T_{comp}$ . Besides, since a differentiator for acceleration observation is adopted in the torque compensation loop, the external noise  $\zeta$  of speed measurement should be considered [11, 12] and the conventional model of WTS is then depicted in Fig. 3.

### 2.3 Discrete model of torque compensation loop

The differential equations implemented in DCS need to be discretized. The rotational acceleration is commonly obtained by the difference calculation of successive measured speeds. Therefore, the observed acceleration  $\alpha_{comp}$  in the torque compensation loop (marked in Fig. 3) is calculated by:

$$\alpha_{comp}(k) = [\omega_g(k) - \omega_g(k - 1)]/T \tag{6}$$

where  $T$  is the sampling interval of rotational speed which

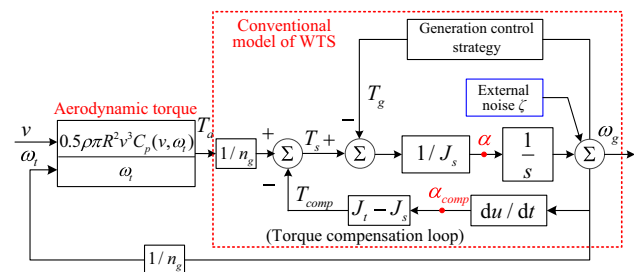


Fig. 3 Block diagram of the WTS with inertia compensation scheme

depends on the fixed-time step of DCS. Likewise, the integral element is discretized as follows:

$$\omega_g(k + 1) = \omega_g(k) + \alpha(k) \cdot T \tag{7}$$

where  $\alpha(k)$  is the average acceleration between two successive sampling points, i.e.,  $kT$  and  $(k + 1)T$ . Substituting (7) into (6), it is obtained that

$$\alpha_{comp}(k) = \alpha(k - 1) \tag{8}$$

This indicates that the one-step time delay, which is irrelevant to the real-time sampling period, is inevitably induced in the discretization process of torque compensation loop. Then, regardless of the nonlinear aerodynamics, the mechanical dynamics of WTS including the one-step time delay and external noise are modeled in Fig. 4a. Similarly, the mechanical dynamics of WT is discretized and illustrated in Fig. 4b. Note that the external noise is not included in the discrete model of WT.

### 3 Analysis on the instability of WTS

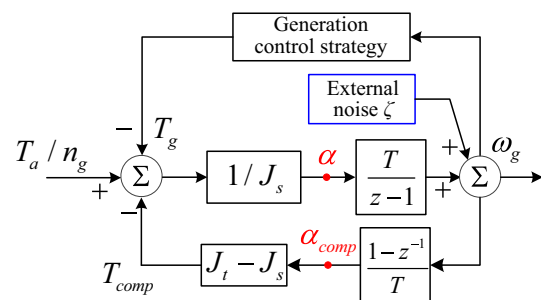
In this section, in order to simplify the stability analysis of WTS, the generator torque is approximated as a linear function of rotational speed, i.e.

$$T_g = k_L \cdot \omega_g \tag{9}$$

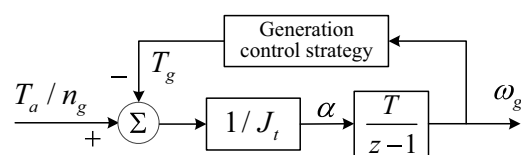
where  $k_L$  is the linearized load factor. Then, the linear time-invariant models of WTS and WT are obtained.

#### 3.1 Stability analysis on the WT model

Regarding the driving torque  $T_a/n_g$  as the input and  $\omega_g$  as the output, the transfer function of the WT model is derived as follows:



(a) Mechanical dynamics of WTS system



(b) Mechanical dynamics of WT system

Fig. 4 Discrete models of mechanical dynamics of WTS and WT

$$H_{real}(z) = \frac{T/J_t}{z + T \cdot k_L/J_t - 1} \tag{10}$$

If the WT is stable, the root of the characteristic equation of (10) should be located in the unit circle. Therefore, the stability condition of WT is obtained as:

$$0 < T \cdot k_L < 2J_t \tag{11}$$

This condition is always satisfied because the magnitude of  $T \cdot k_L$  is much smaller than that of  $J_t$ .

### 3.2 Stability analysis on the WTS model with external noise

Then, this section analyzes the stability of the WTS model in which, as illustrated in Fig. 5, the external noise is considered and the one-step time delay of acceleration observation is neglected by adding a  $z$  element in the torque compensation loop. Correspondingly, the observed acceleration  $\alpha_{comp}$  exactly synchronizes with the real acceleration  $\alpha$  without influencing the generator torque  $T_g$  and the noise  $\zeta$ .

Letting  $T_a/n_g$  be zero input, taking the external noise  $\zeta$  as the input and the compensation torque  $T_{comp}$  as the output, the transfer function of the WTS model shown in Fig. 5 is derived as:

$$H_{wts}^{noise} = \frac{(1 - z^{-1})(J_t - J_s)[(z - 1)/T + k_L/J_s]/J_t}{z + T \cdot k_L/J_t - 1} \tag{12}$$

It can be seen that the characteristic equation of (12) is the same with that of the WT model in (10). This indicates that, so long as the configurations of WT (i.e.,  $T$ ,  $J_t$  and  $k_L$ ) satisfy the stability condition (11), the WTS without the one-step time delay in the acceleration observation is stable even if it is disturbed by the external noise.

### 3.3 Stability analysis on the WTS model considering the one-step time delay

Another model of WTS, which neglects the external noise and considers the one-step time delay, is rebuilt in Fig. 6. Regarding the driving torque  $T_a/n_g$  as the input and

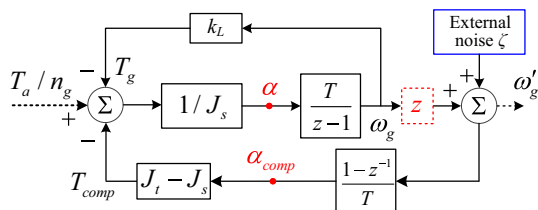


Fig. 5 Discrete model of WTS with the one-step time delay neglected

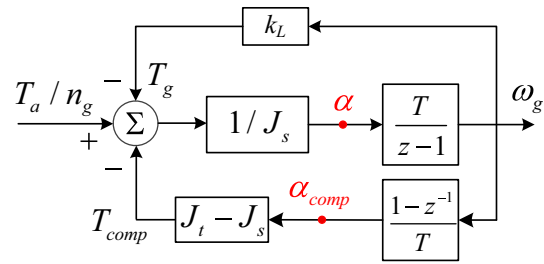


Fig. 6 Discrete model of WTS with the one-step time delay considered

$\omega_g$  as the output, the transfer function of the WTS model shown in Fig. 6 is derived as follows:

$$H_{wts}^{delay} = \frac{T \cdot z}{J_s \cdot z^2 + (T \cdot k_L + J_t - 2J_s) \cdot z + J_s - J_t} \tag{13}$$

Obviously, the characteristic equation of this WTS model is different from that of the WT model because of the one-step time delay. Then, the stability condition of the WTS model considering the one-step time delay is derived by the Routh criterion:

$$J_s > \frac{J_t}{2} + \frac{T \cdot k_L}{4} \tag{14}$$

By comparing (14) with (11), it can be observed that the stability condition of the WTS with time delay becomes relevant to the inertia of WTS  $J_s$ . Moreover, considering that the magnitude of  $T \cdot k_L/4$  is usually much smaller than that of  $J_t/2$ , the stability condition (14) can be simplified as the following formula by omitting the term of  $T \cdot k_L/4$ ,

$$J_t/J_s < 2 \tag{15}$$

According to the above stability analysis, it can be concluded that the instability of WTS is caused by the time delay of acceleration observation rather than external noise. When the inertia  $J_t$  greater than two times  $J_s$  is compensated, the WTS applying the differential-based acceleration observation is unstable even if there is no external noise.

## 4 Improved inertia compensation scheme based on deviation mitigation

Based on the stability analysis of WTS, the deviation of time domain response between WTS and WT resulted from the one-step time delay of acceleration observation is further discussed and mitigated by the improved inertia compensation scheme.

### 4.1 Modeling of response deviation between WTS and WT

The response deviation between WTS and WT is depicted via time domain response analysis. By regarding



the torque difference  $T_a(k)/n_g - T_g(k)$  as the input  $r(k)$  and  $\omega_g(k)$  as the output  $c(k)$ , the open-loop systems of WTS and WT are obtained, as illustrated in Fig. 7 and correspondingly their transfer functions in time domain are derived as follows:

$$c_{wts}(k + 1) - (1 + m) \cdot c_{wts}(k) + m \cdot c_{wts}(k - 1) = n_1 \cdot r(k) \tag{16}$$

$$c_{wt}(k + 1) - c_{wt}(k) = n_2 \cdot r(k) \tag{17}$$

where  $m = (J_s - J_t)/J_s$ ,  $n_1 = T/J_s$  and  $n_2 = T/J_t$  ( $m < 0$ ,  $0 < n_2 < n_1$ ). Let  $r(k)$  be the pulse input and the initial conditions be zero. The pulse responses of the two systems are given as follows:

$$c_{wts}(k) = n_2 \cdot u(k) - \left(\frac{J_s - J_t}{J_s}\right)^k \cdot n_2 \cdot u(k) \tag{18}$$

$$c_{wt}(k) = n_2 \cdot u(k) \tag{19}$$

where  $u(k)$  is the unit step function. By comparing (18) with (19), it is observed that the pulse response of WTS can be decomposed into two response components. The first component is identical with  $c_{wt}(k)$ , while the second one is unexpected and defined as the deviation response:

$$c_d(k) = \left(\frac{J_s - J_t}{J_s}\right)^k \cdot n_2 \cdot u(k) \tag{20}$$

which manifests as an exponential sequence. When  $J_t/J_s \geq 2$ , i.e., the stability condition (15) is not satisfied, the deviation response  $c_d(k)$  is divergent and leads to the instability of WTS. Therefore, only if the divergent deviation  $c_d(k)$  is mitigated, the WTS is stable and replicates the dynamic response similar to WT.

### 4.2 Design of the filter based on deviation mitigation

Note that the deviation response defined in (20) is a regular sequence, which is amplified at each step. According to this law, a first-order digital filter is therefore selected to mitigate the deviation response in discrete time domain and expressed as follows:

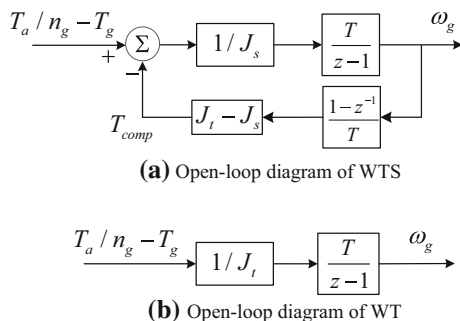


Fig. 7 Open-loop diagram of WTS and WT

$$\hat{c}(k) = \alpha_d \cdot \hat{c}(k - 1) + \beta_d \cdot \hat{r}(k) \tag{21}$$

where  $\hat{r}(k)$  is the input;  $\hat{c}(k)$  is the output,  $\beta_d$  and  $\alpha_d$  are the coefficients of the first-order filter.

While filtering away the deviation response, the designed filter should not modify the expected response component  $c_{wt}(k)$ . Hence, the filter must satisfy the condition that when  $\hat{r}(k) = c_{real}(k)$ ,  $\lim_{k \rightarrow \infty} \hat{c}(k) = \lim_{k \rightarrow \infty} c_{wt}(k)$ .

Then, (21) is rewritten as

$$\lim_{k \rightarrow \infty} \hat{c}(k) = \alpha_d \cdot \lim_{k \rightarrow \infty} \hat{c}(k - 1) + \beta_d \cdot \lim_{k \rightarrow \infty} \hat{r}(k) \tag{22}$$

Assuming that  $\lim_{k \rightarrow \infty} c(k - 1) = \lim_{k \rightarrow \infty} c(k)$ , it is obtained that:

$$\lim_{k \rightarrow \infty} c_{wt}(k) = \alpha_d \cdot \lim_{k \rightarrow \infty} c_{wt}(k) + \beta_d \cdot \lim_{k \rightarrow \infty} c_{wt}(k) \tag{23}$$

Dividing out  $\lim_{k \rightarrow \infty} c_{wt}(k)$  on both sides of (23), a constraint for the coefficients of the filter is derived from (23):

$$\beta_d = 1 - \alpha_d \tag{24}$$

Therefore, the expression of the filter can be rewritten as:

$$\hat{c}(k) = \alpha_d \cdot \hat{c}(k - 1) + (1 - \alpha_d) \cdot \hat{r}(k) \tag{25}$$

Using  $z$  transform, the transfer function of the first-order filter for deviation mitigation is then obtained:

$$H_d(z) = \frac{z(1 - \alpha_d)}{z - \alpha_d} \tag{26}$$

As illustrated in Fig. 8, the designed first-order filter is added in the torque compensation loop and the open-loop transfer function of WTS is modified as:

$$c'_{wts}(k + 2) - [\alpha_d + m(1 - \alpha_d) + 1] \cdot c'_{wts}(k + 1) + [\alpha_d + m(1 - \alpha_d)] \cdot c'_{wts}(k) = n_1 \cdot [r'(k + 1) - \alpha_d \cdot r'(k)] \tag{27}$$

Then, the pulse response of WTS with zero initial condition is obtained as:

$$c'_{wts}(k) = n_2 \cdot u(k) - (\beta \cdot n_2 + \alpha_d \cdot n_1) \cdot \beta^{k-1} \cdot u(k) = c_{wt}(k) - c'_d(k) \tag{28}$$

where

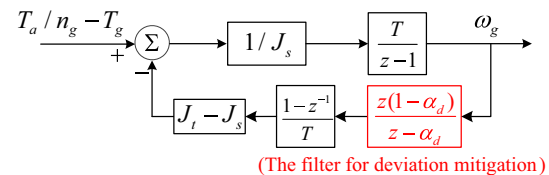


Fig. 8 Open-loop diagram of WTS with the first-order filter employed



$$\beta = \alpha_d + \left( \frac{J_s - J_t}{J_s} \right) \cdot (1 - \alpha_d) \tag{29}$$

It can be inferred from (29) that the pulse response of WTS still consists of two response components. The first one is identical with the expected response  $c_{wt}(k)$ . The second one is a new exponential deviation  $c'_d(k)$ , whose base  $\beta$  is different from that of  $c_d(k)$ . Compared with the base of  $c_d(k)$  determined by the fixed structural parameters (i.e.  $J_t$  and  $J_s$ ), the base of  $c'_d(k)$  is adjustable since the filter coefficient  $\alpha_d$  is introduced. Note that when  $|\beta| < 1$ ,  $\lim_{k \rightarrow \infty} c'_d(k) = 0$ .

That is to say, when  $|\beta| < 1$ , the new deviation is mitigated because it converges to zero with time. According to (29), the convergence condition of  $c'_d(k)$  can be rearranged as

$$\frac{J_t - 2J_s}{J_t} < \alpha_d < 1 \tag{30}$$

Therefore, by employing the first-order filter and setting its coefficient  $\alpha_d$  according to (30), the deviation response  $c'_d(k)$  is mitigated and the pulse response of WTS converges to that of WT. Furthermore, since a complex discrete input can be regarded as a linear weighted combination of pulse signals, the aforementioned pulse response analysis in time domain can be directly extended to the response of WTS excited by a complex input of torque difference.

### 4.3 Stability analysis on WTS with the filter employed

The discrete model of WTS with the first-order filter employed is drawn in Fig. 9 and its closed-loop transfer function is derived as:

$$H_{wts}^{filter} = \frac{T \cdot (z - \alpha_d)}{J_s \cdot z^2 + (k_L T - \beta J_s - J_s) \cdot z + \beta J_s - k_L T \alpha_d} \tag{31}$$

Using the Routh criterion, the stability condition is obtained as:

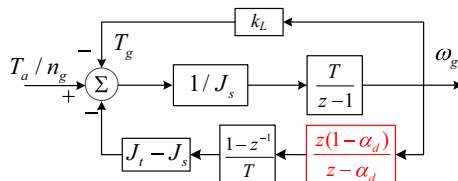


Fig. 9 Discrete model of WTS with the filter employed

$$\frac{J_t - 2J_s + k_L T/2}{J_t - k_L T/2} < \alpha_d < 1 \tag{32}$$

Considering that the magnitude of  $k_L T/2$  is much smaller than that of  $J_t$  or  $J_s$ , the term of  $k_L T/2$  can be omitted. Accordingly, the stability condition of the closed-loop WTS is approximately equivalent to the convergence condition (30) of deviation response  $c'_d(k)$ . Therefore, when the designed filter is applied, the response of WTS is not only stable but also convergent to that of WT.

## 5 Simulation and experimental validation

In this section, the effects of time delay and external noise are comparatively studied by simulations. Then, experiments are conducted to verify the stability of WTS with the proposed inertia compensation scheme.

### 5.1 Simulation studies of WTS

Because electromagnetic response is much faster than mechanical response, a simulation model of WTS, in which the electric system with fast dynamics is neglected, is built in MATLAB/Simulink, as depicted in Fig. 10. The specifications of the simulation model are listed in Table 1. The generator torque is regulated by:

$$T_g = k_{opt} \cdot \omega_g^2 \tag{33}$$

which is a commonly used control strategy for maximum power point tracking (MPPT) of wind turbines, known as the optimal torque control [23].  $k_{opt}$  is the optimal torque gain.

**Simulation case I:** First, the first-order filter is not employed and the simulated moment of inertia  $J_t$  is set to  $3J_s$  (larger than  $2J_s$ ). Additionally, the external noise is not added and a step wind speed is applied as the input. The simulation result plotted in Fig. 11 shows that because the

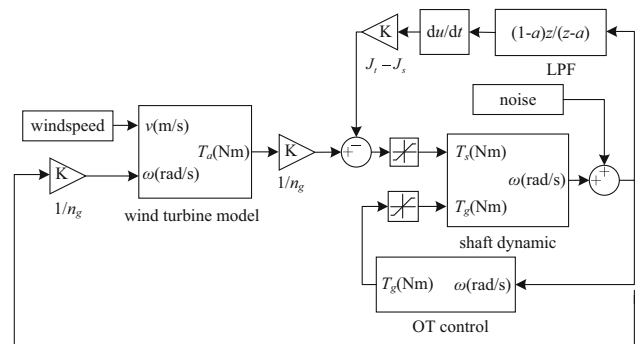
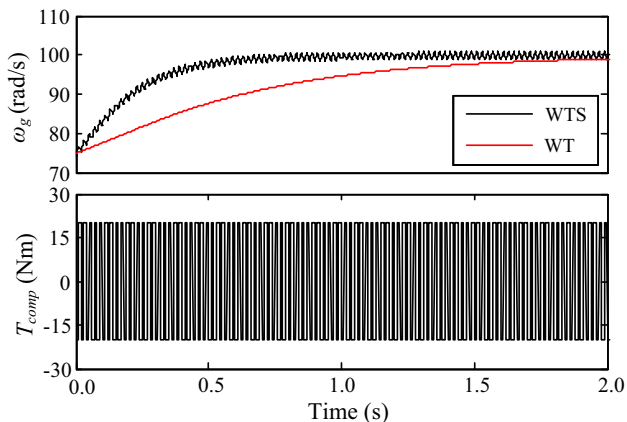


Fig. 10 Simulation model of WTS established in MATLAB/Simulink



**Table 1** The specifications of the simulation model of WTS

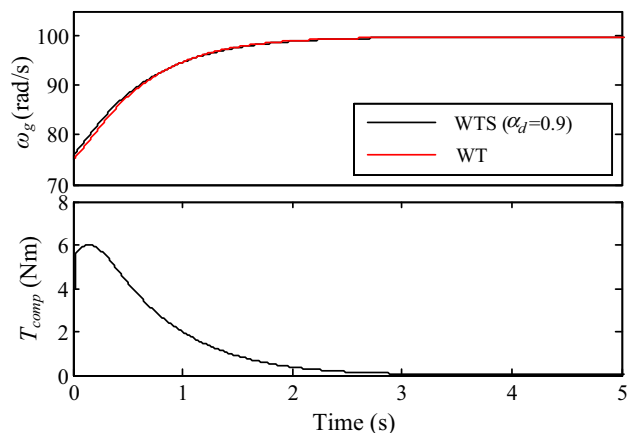
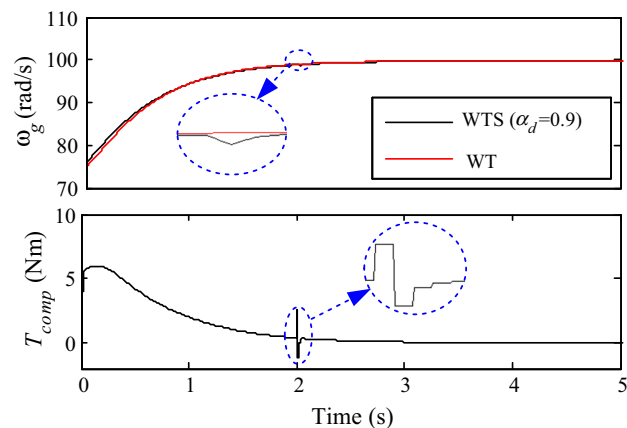
Parameter	Value
Simulation time step	10 ms
Radius of wind turbine, $R$	3.2 m
Maximum power coefficient, $C_{pmax}$	0.311
Optimal tip speed ratio, $\lambda_{opt}$	5.81
Optimal torque gain, $K_{opt}$	0.0071 Nm/(rpm) <sup>2</sup>

**Fig. 11** Simulation case I: WTS without filter and  $J_t$  is set larger than  $2J_s$ 

stability condition is not satisfied, the torque compensation loop is oscillating, which consequently leads to the instability of WTS. It is also validated that when  $J_t$  greater than two times  $J_s$  is compensated, the WTS applying the differential-based acceleration observation is unstable even if there is no external noise, which agrees with the stability condition derived in Section 3. Note that this case cannot be conducted by WTS experiments since signal noise is actually unavoidable.

**Simulation case II:** Then, the first-order filter with  $\alpha_d$  set to 0.9 is utilized and the simulated moment of inertia  $J_t$  remains  $3J_s$ . The value of  $\alpha_d$  satisfies the convergence condition of deviation response expressed as (30). According to the simulation result plotted in Fig. 12, it can be observed that the rotational speed of WTS (black solid line) can stably track that of WT (red solid line) and finally converge to it. This case verifies that by employing the improved inertia compensation scheme based on deviation mitigation, the WTS is able to stably and accurately replicate the dynamic and steady behaviors of WTs.

**Simulation case III:** Next, a pulse noise is added to the rotational speed measurement of WTS at 2s and correspondingly the simulation result is shown in Fig. 13. After the disturbance, the compensation torque immediately converges and the rotational speed of WTS (zoomed in within blue dotted circle) deviates slightly from that of WT (red solid line). It is demonstrated that although the

**Fig. 12** Simulation case II: WTS with filter and  $J_t$  is set larger than  $2J_s$ **Fig. 13** Simulation case III: the speed measurement of WTS is disturbed by a pulse noise at 2s

external noise in rotational speed measurement affects the accuracy of WTS to some extent, it cannot lead to the instability of WTS when the proposed inertia compensation scheme is employed.

**Simulation case IV:** Although WTs with larger  $J_t$  can be stably simulated by increasing  $\alpha_d$ ,  $\alpha_d$  should not be excessively close to 1.0 because of the simulation accuracy of WTS. And in this paper,  $\alpha_d$  is recommended to be smaller than 0.95 in accordance with the discrete time step (10 ms). If  $\alpha_d$  is set too large (e.g., 0.98), the amplitude-frequency response (AFR) of the torque compensation loop at high frequency band is attenuated too much and the transient response of  $T_{comp}$  is slowed down. As a result, the rotational speed of WTS significantly deviates from that of WT though it is stable, as shown in Fig. 14.

## 5.2 System implementation of WTS

The WTS-based WECS in this paper is built according to the structure of practical WECS with full-power

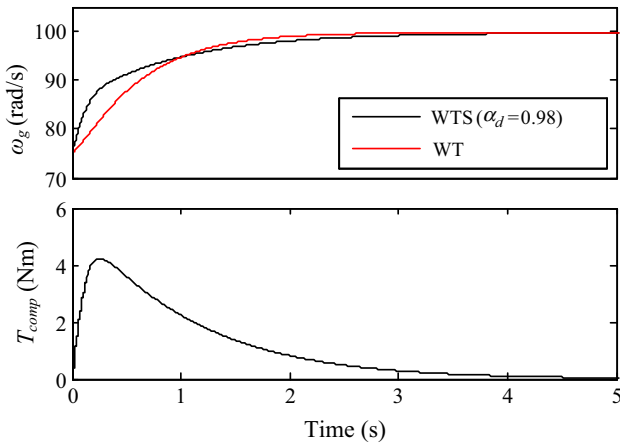


Fig. 14 Simulation case IV: WTS with  $\alpha_d$  set to 0.98

converter where a cascaded control structure through two control loops is commonly adopted [1, 22]:

- 1) The aerodynamic-mechanical part and outer-loop control. The outer-loop control concerns the regulation of wind power generation and provides the generator torque reference as the input to the generator controller (inner-loop control). Because of the slow mechanical behavior of WT, the outer-loop control can be implemented by Programmable Logic Controller (PLC) and its cycle is usually selected as tens of milliseconds.
- 2) The electric part and inner-loop control. The generator control regulates the generator torque according to the torque reference by modulating the rectifier. Besides, the active/reactive power to the grid is regulated by modulating the inverter. Because the electric part and inner-loop control are not discussed in this paper, they are directly accomplished by industrial converters, as commonly implemented in practical WECSs.

The specifications of the WTS test bench designed above are listed in Table 2. Its structure is illustrated in Fig. 15, including the following major components:

- 1) A real-time digital control system (DCS) based on Beckhoff PLC. In DCS, the wind data generation, the acceleration observation, the aerodynamic torque calculation, the proposed inertia compensation scheme and the wind turbine control strategy (i.e., the optimal torque control (33)) are executed every 10ms, and correspondingly the motor torque  $T_s$  and generator torque  $T_g$  are periodically outputted as control references to the motor drive and rectifier.
- 2) A three phase induction motor (IM) driven by a VACON variable-frequency drive. The IM torque is controlled to follow up the torque reference  $T_s$  received from the DCS.
- 3) A permanent magnet synchronous generator (PMSG) coupled with a full-power converter (including a rectifier and an inverter implemented based on VACON drive). The rectifier receives and executes the generator torque  $T_g$ . The inverter regulates the dc-link voltage according to the voltage reference which is set to a constant value.
- 4) A host computer for recording experimental data.

### 5.3 Experimental validation

To test the stability and effectiveness of WTS applying the proposed inertia compensation scheme, the following experimental cases excited by a step wind speed or turbulence are conducted:

**Experimental case I:** First, the first-order filter is not employed and the simulated moment of inertia  $J_t$  is set to the value of  $3J_s$ . As plotted in Fig. 16, the severe oscillation of the compensation torque and rotational speed

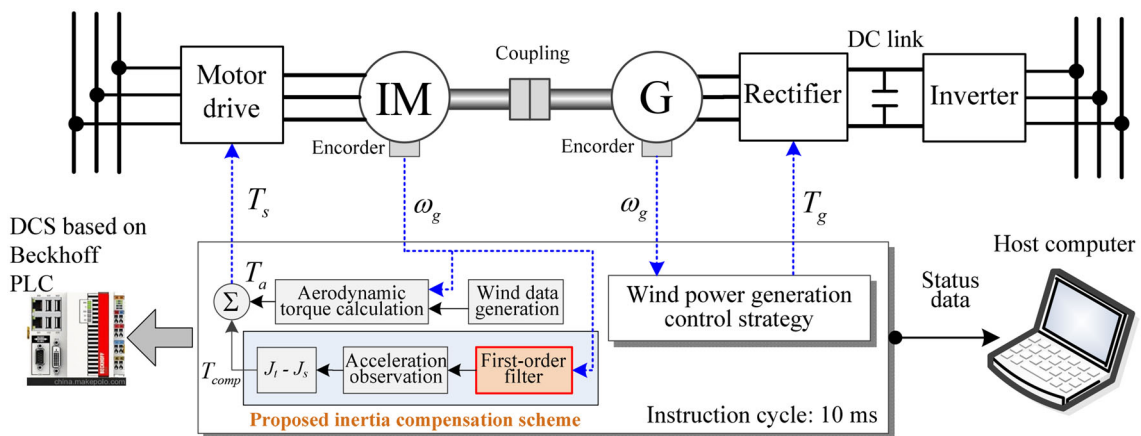
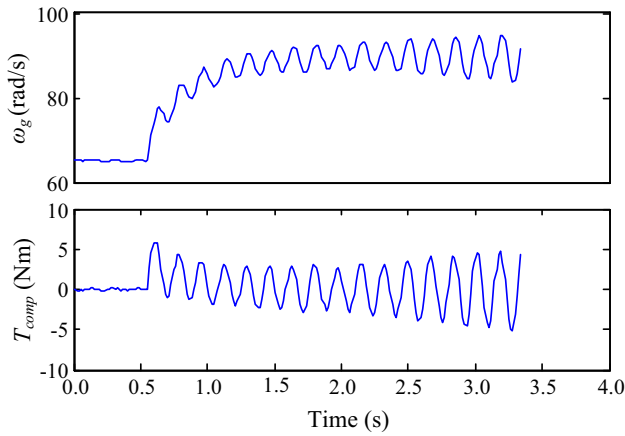


Fig. 15 Hardware structure of the WTS-based WECS



**Table 2** The specifications of the WTS test bench

Parameter	Value
Nominal power of simulated WT	10 kW
Nominal power of IM	15 kW, 1500 RPM
Nominal power of PMSG	10 kW, 1500 RPM
Nominal current of IM	30 A
Nominal current of PMSG	15.5 A
DC-link voltage	550 V
Cycle of PLC	10 ms



**Fig. 16** Experimental case I: WTS without filter and  $J_t$  is set to  $3J_s$

indicates that the WTS is unstable, which is consistent with the stability condition derived in Section 3. Besides, it needs to be pointed out that the oscillating curves are characterized by an asymptotic divergence rather than a random noise disturbance.

**Experimental case II:** Then, the first-order filter is added in the torque compensation loop and its coefficient is determined as 0.9 that satisfies the convergence condition of deviation response (30). As shown in Fig. 17, the stable trajectories demonstrate that the filter designed for mitigating the deviation response does work and the WTS with  $J_t = 3J_s$  is stabilized.

**Experimental case III:** In order to test the inertia effect of the WTS simulating different values of  $J_t$ , more experiments, in which  $J_t/J_s$  is set at various values (from 1.0 to 5.0) and correspondingly  $\alpha_d$  is adjusted by (30), are carried out. The dynamic responses excited by the same step wind speed are drawn in Fig. 18. It is observed that the rise time gradually increases with the simulated  $J_t$ . Additionally, after the dynamic process, the WTS with different values of  $J_t$  reaches the same rotational speed. Therefore, the inertia effect, especially the slow dynamic behavior due to larger inertia, is stably replicated by applying the proposed inertia compensation scheme.

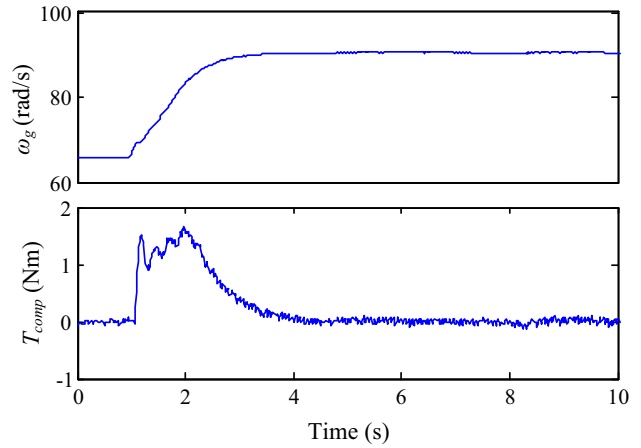


**Fig. 17** Experimental test II: WTS with filter and  $J_t$  is set to  $3J_s$

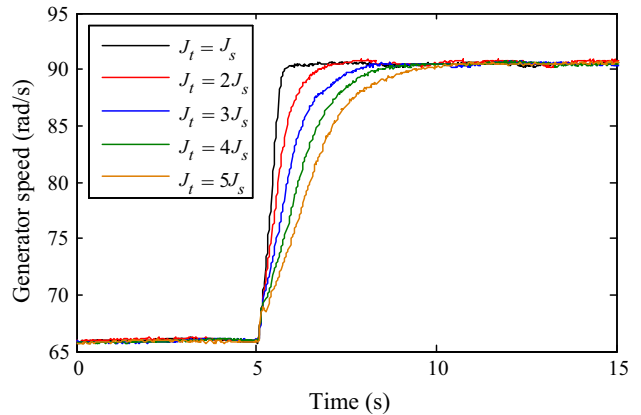


**Fig. 18** Experiments III: rotational speed trajectories of the WTS with different moment of inertia  $J_t$

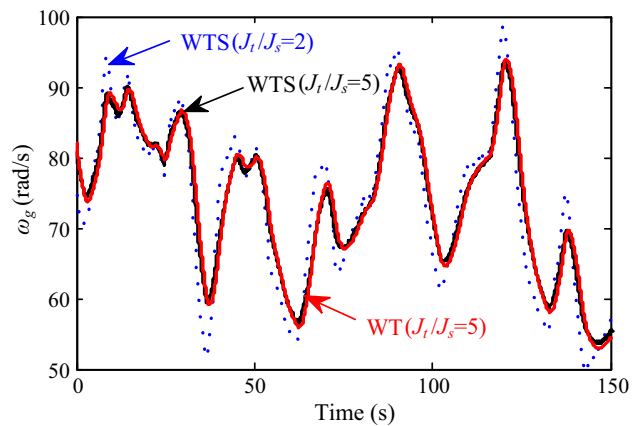


**Fig. 19** Experiments IV: rotational speed trajectories of the WTS and WT in response to turbulence

**Experimental case IV:** Furthermore, the dynamic behavior of WTS with different values of  $J_t$  in response to turbulent wind is compared. As shown in Fig. 19,

the rotational speed trajectories of the WTS differ for  $J_t$ . Moreover, the larger is the moment of inertia  $J_t$  simulated by the WTS, the slower the rotational speed in response to turbulence. In addition, the rotational speed trajectory (red solid line) calculated by the WT model (3) with  $J_t = 5J_s$  is also plotted in Fig. 19. It is apparent from Fig. 19 that for the same moment of inertia  $J_t$ , the rotational speed trajectory of WTS approximates to that of WT. This means that the proposed inertia compensation scheme based on deviation mitigation can replicate the slow mechanical dynamics of large-inertia WTs stably and accurately.

## 6 Conclusion

To verify the control and optimization of WECS, the WTS should reproduce the dynamic behavior similar to WTs. However, the applicability of WTS to simulating large-inertia WTs is limited by the instability of WTS. In this paper, the instability of WTS applying the inertia compensation scheme is analyzed and interpreted as the consequence of the one-step time delay of acceleration observation. By establishing the linear discrete model of WTS considering time-delay and analyzing its stability condition, an inertia compensation scheme, in which a first-order filter for eliminating deviation response is added to the torque compensation loop, is proposed for stabilizing WTS. Without changing the inner loop control and experimental hardware, the WTS-based test bench can conveniently and economically implement the proposed inertia compensation scheme and reproduce the slow mechanical dynamics of WTs.

**Acknowledgment** This work is supported by National Natural Science Foundation of China (No. 61203129, No. 61174038, No. 51507080), Jiangsu Planned Projects for Postdoctoral Research Funds (No. 1301014A) and the Fundamental Research Funds for the Central Universities (30915011104).

**Open Access** This article is distributed under the terms of the Creative Commons Attribution 4.0 International License (<http://creativecommons.org/licenses/by/4.0/>), which permits unrestricted use, distribution, and reproduction in any medium, provided you give appropriate credit to the original author(s) and the source, provide a link to the Creative Commons license, and indicate if changes were made.

## References

- [1] Boukhezzer B, Siguerdidjane H (2011) Nonlinear control of a variable-speed wind turbine using a two-mass model. *IEEE Trans Energy Convers* 26(1):149–162
- [2] Rajendran S, Jena D (2014) Variable speed wind turbine for maximum power capture using adaptive fuzzy integral sliding mode control. *J Mod Power Syst Clean Energy* 2(2):114–125. doi:10.1007/s40565-014-0061-3
- [3] Li J, Zhang X-P (2016) Impact of increased wind power generation on subsynchronous resonance of turbine-generator units. *J Mod Power Syst Clean Energy* 4(2):219–228. doi:10.1007/s40565-016-0192-9
- [4] Li H, Steurer M, Shi KL et al (2006) Development of a unified design, test, and research platform for wind energy systems based on hardware-in-the-loop real-time simulation. *IEEE Trans Ind Electron* 53(4):1144–1151
- [5] Park K, Lee KB (2010) Hardware simulator development for a 3-parallel grid-connected PMSG wind power system. *J Power Electron* 10(5):555–562
- [6] Wang JQ, Ma YD, Hu ZR et al (2009) Modeling and real-time simulation of non-grid-connected wind energy conversion system. In: *Proceedings of the 2009 world non-grid-connected wind power and energy conference*, Nanjing, China, 24–26 Sept 2009, 5 pp
- [7] Dolan DSL, Lehn PW (2005) Real-time wind turbine emulator suitable for power quality and dynamic control studies. In: *Proceedings of the international conference on power systems transients (IPST'05)*, Montreal, Canada, 19–23 June 2005, 6 pp
- [8] Abo-Khalil AG (2011) A new wind turbine simulator using a squirrel-cage motor for wind power generation systems. In: *Proceedings of the 9th international conference on power electronics and drive systems (PEDS'11)*, Singapore, 5–8 Dec 2011, pp 750–755
- [9] Kojabadi HM, Chang LC, Boutot T et al (2004) Development of a novel wind turbine simulator for wind energy conversion systems using an inverter-controlled induction motor. *IEEE Trans Energy Convers* 19(3):547–552
- [10] LI WJ, Yin MH, Zhou R et al (2015) Investigating instability of the wind turbine simulator with the conventional inertia emulation scheme. In: *Proceedings of the 2015 IEEE energy conversion congress and exposition (ECCE'15)*, Montreal, Canada, 20–24 Sept 2015, pp 983–989
- [11] Chen JW, Chen J, Gong CY et al (2012) Design and analysis of dynamic wind turbine simulator for wind energy conversion system. In: *Proceedings of the 38th annual conference on IEEE Industrial Electronics Society (IECON'12)*, Montreal, Canada, 25–28 Oct 2012, pp 971–977
- [12] Chen J, Chen JW, Chen R et al (2011) Static and dynamic behaviour simulation of wind turbine based on PMSM. *PCSEE* 31(15):40–46
- [13] Liu Y, Zhou B, Guo HH et al (2014) Static and dynamic behaviour emulation of wind turbine based on torque PDF. *Trans China Electrotech Soc* 29(11):116–125
- [14] Guo HH, Zhou B, Liu Y et al (2013) Static and dynamic behaviour emulation of wind turbine based on load torque observation. *PCSEE* 33(27):145–153
- [15] Chen J, Gong CY, Chen JW et al (2012) Comparative study of dynamic simulation methods of wind turbine. *Trans China Electrotech Soc* 27(10):79–86
- [16] Neammanee B, Sirisumrannukul S, Chatratana S (2007) Development of a wind turbine simulator for wind generator testing. *Int Energy J* 8(1):21–28
- [17] Munteanu I, Bratcu AI, Bacha S et al (2010) Hardware-in-the-loop-based simulator for a class of variable-speed wind energy conversion systems: design and performance assessment. *IEEE Trans Energy Convers* 25(2):564–576
- [18] Gong B, Xu DW (2008) Real time wind turbine simulator for wind energy conversion system. In: *Proceedings of the IEEE power electronics specialists conference (PESC'08)*, Rhodes, Greece, 15–19 Jun 2008, pp 1110–1114



- [19] Monfareda M, Kojabadib HM, Rastegara H (2008) Static and dynamic wind turbine simulator using a converter controlled dc motor. *Renew Energy* 33(5):906–913
- [20] Camblong H, Alegria IMD, Rodriguez M et al (2006) Experimental evaluation of wind turbines maximum power point tracking controllers. *Energy Convers Manag* 47(18/19):2846–2858
- [21] Nichita C, Luca D, Dakyo B et al (2002) Large band simulation of the wind speed for real time wind turbine simulators. *IEEE Trans Energy Convers* 17(4):523–529
- [22] Boukhezzer B, Siguerdidjane H (2009) Nonlinear control with wind estimation of a DFIG variable speed wind turbine for power capture optimization. *Energy Convers Manag* 50(4):885–892
- [23] Abdullah MA, Yatim AHM, Tan CW et al (2012) A review of maximum power point tracking algorithms for wind energy systems. *Renew Sustain Energy Rev* 16(5):3220–3227

**Weijie LI** received the B.Eng. degree in electrical power engineering from Nanjing University of Science and Technology, Nanjing, China, in 2013. He is currently working toward the M.Eng. degree in smart grid technology and control at Nanjing University of Science and Technology. His research interests include wind power conversion system and smart grid.

**Minghui YIN** received the B.Eng. and M.Eng. degrees in electrical power engineering and Ph.D. degree in control science and

engineering from Nanjing University of Science and Technology, Nanjing, China, in 1999, 2002 and 2009, respectively. He was a Research Assistant with the Department of Electrical Engineering, The Hong Kong Polytechnic University, Hong Kong, from July 2007 to July 2008. Since 2009, he has been with the Joint Research Centre for Smart Grid Technology and Control, School of Automation, Nanjing University of Science and Technology, where he is currently an Associate Professor. His major research interests include wind power conversion system, power system economic operation and power system transient stability.

**Zaiyu CHEN** received the B.S. degree in mathematics from Nanjing University of Science and Technology, Nanjing, China, in 2012. He is currently working toward the Ph.D. degree in control science and engineering at Nanjing University of Science and Technology. His research interests include wind power conversion system.

**Yun ZOU** was born in 1962. He received the B.S. degree in mathematics from the Northwestern University, Xi'an, China, in 1983, and the M.S. and Ph.D. degrees in control theory and control engineering from Nanjing University of Science and Technology, Nanjing, China, 1987, and 1990, respectively. He is currently a professor in the School of Automation, Nanjing University of Science and Technology. His current research interests include differential-algebraic equation systems, two-dimensional systems, singular perturbations, transient stability of power systems, and power market.